TETHERED CHAINS IN CONCAVE VOLUMES. A MONTE CARLO STUDY

Karel PROCHAZKA and Zuzana LIMPOUCHOVA

Department of Physical and Macromolecular Chemistry, Charles University, 128 40 Prague 2, The Czech Republic

Received May 4, 1994
Accepted June 27, 1994

Monte Carlo study of tethered chain conformations in spherical cavities was performed in a relatively broad range of average segment densities (i.e. numbers of tethered chains with increasing length in the sphere). Simulations were performed on a tetrahedral lattice using (i) an equilibrated self-avoiding walk for systems containing a single tethered chain with increasing length, and (ii) a simultaneous self-avoiding walk of many tethered chains in the spherical cavity together with equilibration of the system which was performed by a modified algorithm similar to that of Siepmann and Frenkel. Only a geometric excluded volume effect of segments was considered (i.e. the prohibition principle of a double occupancy of one lattice site by two different segments). Various distribution functions (e.g. distribution of the end-to-end and the end-to-gravity center distances and their orientations with respect either to the radial direction, or to the direction of the first-to-second segment connection, etc.) were calculated and the effect of increasing average segment density in the sphere on conformational characteristics of individual chains was studied. It was found that conformational and orientational properties of relatively short tethered chains are only little affected by increasing segment density (i.e. by the number of chains in the spherical cavity), whereas arrangements of long tethered chains are significantly influenced by the density of the system.

A reliable and detailed knowledge of conformational properties of tethered chains is extremely important for a proper understanding of many processes in physical chemistry of macromolecules, such as sorption of polymers on various surfaces[1,2], behavior of highly branched polymeric "stars"[3,4], or block copolymer micelles in selective solvents[5,6] and relaxation processes in systems containing polymeric brushes[7–10]. One class of very useful methods for studying those systems are Monte Carlo and molecular dynamics simulations[11–19]. Despite an intense and concentrated interest of theoreticians in various tethered chain systems, Monte Carlo studies on tethered chains in small closed volumes are practically nonexistent.

In our recent papers[20–23], we have started a systematic study of the behavior of dense systems of tethered chains in restricted volumes. The main objectives of our investigation were aimed: (i) to elucidate the conformational behavior of insoluble blocks in cores of multimolecular micelles in selective solvents, and (ii) to simulate various fast photophysical processes which proceed in those systems[24–29]. In order to simulate

properties of realistic micellar cores, we have studied systems of relatively long chains at relatively high segment densities.

During our simulations, we have met several interesting problems which are important for a general understanding of thermodynamic properties of tethered chain systems in restricted geometries and for a correct interpretation of results of our simulation procedure, in spite of the fact that they do not fit into the scheme of the intended studies of photochemical processes in realistic micellar cores. In this communication we report on two of those problems.

The first one examines a general relationship between properties of an isolated tethered chain in a closed spherical volume and the corresponding dense multi-chain systems. The latter topic concerns the practical applicability, (i.e. the reliability and the speed of the equilibration procedure, etc.) of a simultaneous multi-chain self-avoiding walk algorithm at high segment densities and scrutinizes the physical significance of results at the very limit of its feasibility.

When considering the first topic, the following questions arise:

a) Are certain features of the conformational behavior of an isolated tethered chain in a constrained geometry partially conserved in dense systems of many tethered chains under the same geometrical constraints?

b) How is the "memory of the single chain behavior" at various segment densities influenced by the ratio, $\xi = Ll/R$ ("the external constraint parameter", ξ). Parameter ξ represents the relative curvature of the surface with respect to the chain length and gives a quantitative measure of the strength of external geometrical constraints (L is the number of segments of the length l, and R is the radius of the spherical cavity)?

c) Does there exist a certain shift towards "the ideal chain behavior" at high densities (caused by the presence of many other chains) which is known in dense systems of free (i.e. non-tethered) chains[30,31]?

The second topic concerns the behavior of dense systems. All variants of simulation techniques based on the self-avoiding walk do not work well at high densities[12,13]. It is therefore necessary to investigate the physical meaning of the data and the general reliability of the used simulation algorithm.

In this communication we study changes in various conformational distribution functions with increasing chain length in a broad range of average segment densities for systems of tethered chains in relatively small spherical volumes. This enables us to answer (at least partially) the above formulated questions.

METHOD

Simulation Procedure

Principles of the simulation technique have been described in details in our previous papers[20–22]:

1. For systems containing a single tethered chain with increasing number of segments, L, it is the self-avoiding walk on a tetrahedral lattice (with a distance l of the lattice sites) in a restricted volume with the Rosenbluth weights[32] and a modified Metropolis acceptance rule[33]. The self-avoiding walk starts at a randomly chosen point in a narrow surface layer. Distribution functions are calculated on the basis of $\approx 10^6$ statistically uncorrelated conformations.

2. Simulation for multi-chain systems proceeds as follows: (i) Conformations of N tethered chains (each containing L segments) in a restricted spherical volume are generated by the simultaneous self-avoiding walk on a tetrahedral lattice. All chains start in a narrow spherical surface layer. "Thermal equilibration" of the system, which is necessary to remove the bias of the steadily increasing density of the occupied lattice sites during the simultaneous growth of many chains and to circumvent the "attrition problem"[13] and to correct its consequences, proceeds in two steps: (ii) A randomly chosen chain is disregarded and a new chain is grown again in the dense system from a random surface site. This step is repeated ($N^2/2$) times. (iii) To reach the equilibrium of the system, the step (ii) is repeated again ($N^2/2$) times and the Rosenbluth weights, $w_i^{(k)}$, in each step, i, and the total weights of resulting chain conformations, k, $W_k = \prod_{i=1}^{L} w_i^{(k)}$, are evaluated, ($w_1^{(k)} = 1$, $k = 1,2$, for the old and the new conformation, respectively). The new conformation of a chain is accepted according to a modified Metropolis criterion for the factor (W_{new}/W_{old}). The system consisting of the last N accepted chains is considered as one statistically uncorrelated multi-chain conformation which represents a randomly chosen micellar core from the thermally equilibrated micellar system.

The simulation procedure is a specific modification of the algorithm proposed by Siepmann and Frenkel[34] for dense polymer systems. It is a suitable simulation technique for systems of tethered chains[20–22]. We have tested also the three-bonds "crankshaft" motion (a modification of the Verdier algorithm[35]) in the studied system, but the latter was relatively slowly convergent and thus much less efficient than the previous one.

In this paper, we consider only the geometrical excluded volume effect of segments which plays more important role in dense systems (and mainly in dense constrained systems) than relatively small additional attractive, or repulsive interactions between individual polymer segments and solvent molecules[31,36].

The presented distributions were calculated on the basis of $\approx 10^4$ statistically uncorrelated multi-chain arrangements. The simulation of each multi-chain arrangement starts by a totally independent simultaneous self-avoiding walk and continues by the above described equilibration of the system, which represents a generation of N^2 new chain arrangements (generally $\approx 10^4$ to 10^5 segment positions). It means that the data are based on $\approx 10^8$ to 10^9 successfully generated segment positions.

Simulations for highly dense systems (a fraction of the occupied lattice sites ≈ 0.6 and higher) were modified in the following way: In dense systems, the most time-con-

suming procedure is the simultaneous self-avoiding walk which creates the starting multi-chain arrangement for further equilibration of the system. In that case, only a very low fraction of generated segment positions in the constrained multi-chain system, $\approx 10^{-3}$, are accepted. To accelerate our simulations, we have performed a simultaneous self-avoiding walk with a bit shorter chains containing $(L - m)$ segments. We have used $m \in \langle 1,22 \rangle$ to test the speed and convergency of this simulation variant. All chains were one by one disregarded and grown again up to the length L. Then steps (ii) and (iii) of the above described equilibration were used to equilibrate the studied system. Simulations using this modification in a broad range of segment densities have shown that the equilibrated data are identical with those presented earlier. In contrast to the original simulation technique, the upgraded variant may be successfully used for elevated segment densities in a reasonable time.

Physical nature of the problem does not require to use the periodic boundary conditions.

Calculations were performed on a DEC 5000/200 computer. Programs were written in FORTRAN 77. The longest calculations took up to several weeks of the CPU.

Calculated Distribution Functions

All functions presented in this communication were constructed as histograms during simulations of many individual chain conformations:

a) Distribution of the tethered end-to-free end distances of individual chains, $\rho_{TF}(r_{TF})$, corresponds to the probability that the free end of a chain is located in the distance r_{TF} from the tethered end which is placed in a narrow spherical surface layer of the thickness, $\Delta_S = 0.1\ l$. Distribution, $\rho_{TF}(r_{TF})$, was calculated as follows: A chain configuration is created inside the spherical cavity and a system of narrow concentric layers is drawn around the tethered end in the cavity (see Fig. 1). If the free end falls

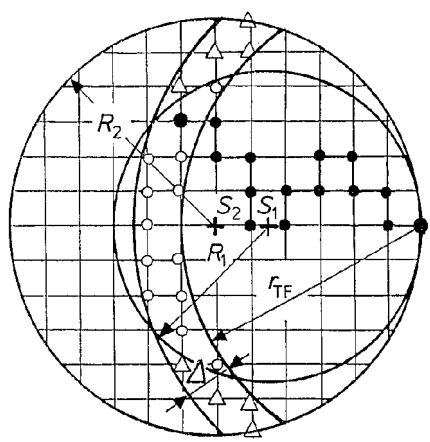

FIG. 1
A two-dimensional scheme explaining the evaluation of the distribution function, $\rho_{TF}(r_{TF})$, of the tethered end-to-free end distances, r_{TF}. Function $\rho_{TF}(r_{TF})$ is constructed as a histogram on the basis of numbers of end-points of individual chains which fall during simulations into narrow semispherical layers with increasing radius r_{TF} and a constant thickness, $\Delta = 1.25\ l$, drawn around the position of the tethered end of a chain. They are normalized by the total number of all generated chains, M_{tot}, and by numbers, N_r, of lattice sites in corresponding layers (averaged over all possible positions of the tethered ends in a narrow spherical surface layer of the thickness, $\Delta_S = 0.1\ l$). Numbers N_r increase for a constant r_{TF} with increasing R

into a narrow concentric layer of the radius, r_{TF}, and a width, $\Delta = 1.25\ l$, the value $1/N_r$ is added to the value of the calculated function corresponding to r_{TF} (N_r is the number of all lattice sites in that particular layer). Values N_r are averaged over all possible locations of tethered ends in a narrow spherical surface layer of the thickness, $\Delta_S = 0.1\ l$. The calculated distribution is then constructed as a histogram based on the total number of chain conformations, M_{tot}, $\approx 10^6 - 10^7$, and normalized by M_{tot}. Numbers N_r for constant r_{TF} increase with increasing radius of the cavity, R. Magnitudes of $\rho_{TF}(r_{TF})$ generally decrease with increasing R since the normalization factor, $M_{tot}\ N_r$, is R-dependent. Strictly speaking, distribution, $\rho_{TF}(r_{TF})$, is a probability density function.

b) Distribution functions, $\rho_{TC}(r_{TC})$, and $\rho_{FC}(r_{FC})$, of the tethered end-to-gravity center, and the free end-to-gravity center distances, respectively, are calculated similarly to the $\rho_{TF}(r_{TF})$ distribution.

c) Number distributions of the end-to-end distances, $n_{TF}(r_{TF})$, or the end-to-gravity center distances, $n_{TC}(r_{TC})$ and $n_{FC}(r_{FC})$, are the number fractions of chains with distances r_{TF}, r_{TC} and r_{FC}, respectively. They are not normalized by numbers of the lattice sites in semispherical layers. Some of them are shown together with the ρ-functions to give a better picture of the behavior of the system since it is not easy for a reader to recalculate without other information the ρ-functions into the corresponding *n*-functions.

d) Angular distribution of orientations of the end-to-end vectors (i.e. the tethered end-to-free end vectors, $\psi_{TF}^{(r)}(\vartheta)$), with respect to the radial direction, and distribution of orientations of the tethered end-to-gravity center vectors, $\psi_{TC}^{(r)}(\vartheta)$, are normalized by M_{tot} and by numbers of all lattice sites in volume elements confined between two cones with a common apex at the surface (an inner angle ϑ, and the outer angle, $\vartheta + \Delta\vartheta$), see Fig. 2. Similarly to the evaluation of the ρ-functions, the normalization numbers, N_ϑ, are averaged over all possible apex location in the surface layer of the thickness, $\Delta_S = 0.1\ l$. Number fractions of chains with particular orientations of the end-to-end, $\boldsymbol{r}_{TF}$, or end-

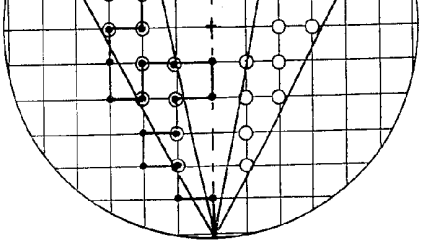

FIG. 2
A two-dimensional scheme explaining the evaluation of the angular distribution function of the end-to-end vectors, $\boldsymbol{r}_{TF}$, with respect to the radial direction, $\psi_{TF}^{(r)}(\vartheta)$. Values of $\psi_{TF}^{(r)}(\vartheta)$ are normalized by the total number of all generated chains, M_{tot}, and by numbers of the lattice sites, N_ϑ, in small volume elements, ΔV_ϑ, confined between two cones with a common apex which is defined by the tethered end position. Apex angles of the inner and the outer cone are 2ϑ and $2(\vartheta + \Delta\vartheta)$, respectively, with $\Delta\vartheta = 5°$. Numbers, N_ϑ, are averaged over all possible positions of the tethered ends of chains and for constant ϑ, they increase with increasing R

to-gravity center vectors, $\boldsymbol{r}_{TC}$ and $\boldsymbol{r}_{FC}$ (not normalized by N_ϑ numbers), i.e. $n_{TF}^{(r)}(\vartheta)$, $n_{TC}^{(r)}(\vartheta)$ and $n_{FC}^{(r)}(\vartheta)$, are also shown in some figures. In case of orientations of the free end-to-gravity center vectors, only functions $n_{FC}^{(r)}(\vartheta)$ are discussed for the reasons that are given in ref.[22].

e) Angular distribution function of orientations of the end-to-end vectors with respect to the orientation of the first-to-second segment connection, $\psi_{TF}^{(12)}(\varphi)$, is calculated similarly to the previous function.

f) Number fractions of projections of various vectors into either the radial direction (e.g. $f_{TF}^{(r)}$ ($p_{TF}^{(r)}$), etc.), or the direction of the first-to-second segment connection (i.e. $f_{TF}^{(12)}$ ($p_{TF}^{(12)}$)) are counted directly during simulations (see Fig. 3).

g) Distribution of the radii of gyration, $g_R(R_g)$, was calculated immediately after evaluation of R_g values of individual chains.

h) Two other functions, $g_S^{(C)}(r_{CS})$ and $n_{FC}^{(TC)}(\omega)$, were calculated to broaden the description of the system behavior. Function $g_S^{(C)}(r_{CS})$ is the density of segments of a particular chain around its gravity center (i.e. in the distance r_{CS} from the center). That function is normalized by numbers of the lattice sites in narrow concentric spherical layers with the origin in the gravity center, which are located inside the considered cavity. Function $n_{FC}^{(TC)}(\omega)$ is the angular distribution of mutual orientations of $\boldsymbol{r}_{FC}$ and $\boldsymbol{r}_{TC}$ vectors (i.e. the number fractions of chains, $\boldsymbol{r}_{FC}$ and $\boldsymbol{r}_{TC}$ of which form angles ω).

RESULTS AND DISCUSSION

Low Density Limit

Distributions of the End-to-End and the End-to-Gravity Center Distances

In our systematic study of constrained tethered chain systems, we have gathered a large collection of simulated data on the behavior of those systems under various conditions.

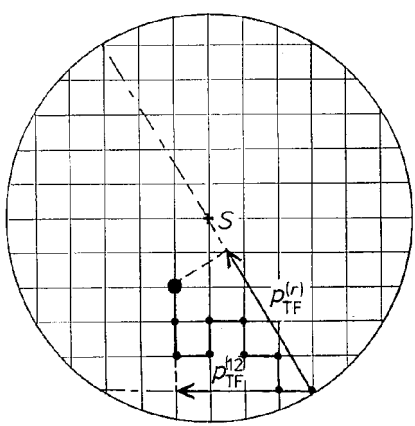

FIG. 3
A two-dimensional scheme explaining the evaluation of projections of the end-to-end vectors, $\boldsymbol{r}_{TF}$, into the radial direction and into the direction of the first-to-second segment connection

Those conditions are given by various combinations of the cavity radii, numbers of chains and their lengths and may be characterized by two principal parameters: the average segment density, $\langle g_S \rangle = NL/N_{tot}$ (where N_{tot} denotes the total number of lattice sites in the cavity), and the constraint parameter, $\xi = Ll/R$. However, those parameters alone do not determine unambiguously all properties of the system. It is absolutely impossible to show all dependences of calculated functions on all variables which would be interesting to discuss in this paper. We have chosen a relatively large collection of simulated data and we try to show the most important trends. This collection proves the consistency of the data and enables us to get maximum information on the system behavior in a broad range of conditions. Many curves and their dependences on various variables are not shown, but only described and discussed. Sometimes we make references to our previous papers[20–22] and even to certain particular figures which are shown therein.

At first, we discuss the simulated distributions of the end-to-end distances (i.e. the tethered end-to-free end distances) for single chains with increasing length (number of segments, L) in spherical cavities with three different radii, R. We have chosen the same basic set of combinations of L and R values as in our previous papers[21,22] and added several smaller and bigger values of L to broaden the relative range of the chain lengths in some figures, where we have felt that it might help to assess general principles of the constrained systems behavior. Figure 4*a* – 4*c* show the end-to-end distribution function, $\rho_{TF}(r_{TF})$, for a single tethered chain of increasing length, L, in three different cavities.

A comparison of curves for various systems shows an increasing effect of external geometrical constraints on the chain conformations with increasing value $\xi = Ll/R$. Distributions, $\rho_{TF}(r_{TF})$, for less constrained tethered chains (i.e. for almost "non-compressed chains" with a low ξ) rise steeply with increasing r_{TF} (in the region of small r_{TF}), reach well-pronounced maxima for $r_{TF} < R$ (depending on L), and then decay fast to zero for $r_{TF} > R$. The decay parts are evidently S-shaped. With increasing ξ, the shape and symmetry of distribution functions, $\rho_{TF}(r_{TF})$, changes dramatically. Curves for large ξ rise relatively slowly and reach very flat maxima around $r_{TF} \approx (3/2)R$. They drop fast for $r_{TF} \to 2R$. The drop for large r_{TF} is concave and faster than the rise in the region of small r_{TF}.

Curves for small ξ are similar to distributions for an isolated self-avoiding chain[30,31]. It suggest that in case of less constrained systems, the tethered chain may adopt with a high probability conformations quite similar to those of an isolated free chain. The only significant exception is the loss of the spherical symmetry of possible chain orientations in space with respect to the tethered end. Such a situation may preferentially take place if the most probable end-to-end distance for the free chain of a given length and the distance, for which the normalization factor, N_r, reaches a maximum value, are identical (see Fig. 1). The sum of products of numbers of lattice points in the distance r_{TF} (i.e.

number of possible locations of chain ends) and corresponding numbers of different paths how to reach them in L steps from a fixed tethered end determines the probability of all conformations with a particular r_{TF} value in dilute athermal system of constrained tethered chains.

Figure 5*a* shows that distributions, $\rho_{TF}(r_{TF})$, for low L – i.e. for low ξ (solid curves *1* – *3*) are similar to each other – they depend on L only, but not at all on R. Maxima are reached for the same r_{TF} values. Their different magnitudes are caused by the R-dependent normalization factor (cf. Fig. 1). The situation is quite different for high L – i.e. for high ξ (dashed curves *4* – *6*) and the character of individual curves changes significantly with increasing R. The shape of the distribution function, $\rho_{TF}(r_{TF})$, for L = 93 and the highest R = 15 l (for a relatively lower value of ξ – curve *6*) is again similar to curves *1* – *3*.

The end-to-end distribution functions, $\rho_{TF}(r_{TF})$, for increasing numbers of tethered chains, N, in the smallest spherical cavity (i.e. for increasing average segment density, $\langle g_S \rangle$, within the sphere with a radius, R = 10 l) are shown in Fig. 5*b* (solid curves for relatively short chains, L = 31 and dashed curves for long chains, L = 93). Three findings are of interest:

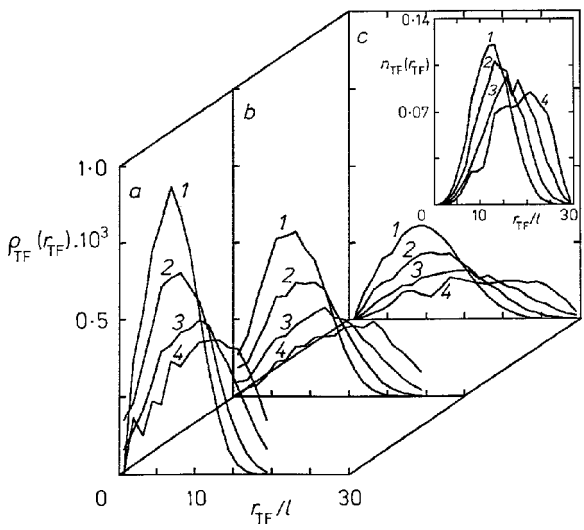

FIG. 4

Distribution function of the tethered end-to-free end distances, $\rho_{TF}(r_{TF})$, for single tethered chains with increasing number of segments, L, in three spherical cavities with increasing radius, R: *a* R = 10 l; L = 31 (*1*), L = 40 (*2*), L = 56 (*3*), L = 93 (*4*); *b* R = 12.5 l; L = 40 (*1*), L = 52 (*2*), L = 72 (*3*), L = 119 (4); *c* R = 15 l; L = 55 (*1*), L = 71 (*2*), L = 99 (*3*), L = 163 (*4*); insert in Fig. 4*c*: number fractions, $n_{TF}(r_{TF})$, of chains with end-to-end distances, r_{TF}, corresponding to $\rho_{TF}(r_{TF})$ in Fig. 4*c*

a) Distributions for less constrained chains, $\xi = 3.1$, i.e. for relatively short ones (solid curves), do not change significantly in a broad range of chain numbers, $N \in \langle 1,45 \rangle$ (i.e. for average segment densities, $\langle g_S \rangle \in \langle 0.01 - 0.51 \rangle$, in a sphere with $R = 10\ l$). The only observable change is a small shift in maxima positions towards lower r_{TF} value with increasing number of chains, N.

b) For systems with relatively long chains (strongly constrained systems with a high $\xi = 9.3$), shapes of dashed curves change completely with increasing number of chains, $N \in \langle 1,20 \rangle$, which corresponds to $\langle g_S \rangle \in \langle 0.03 - 0.68 \rangle$. At high segment densities, distributions of the end-to-end distances, $\rho_{TF}(r_{TF})$, for long tethered chains in constrained systems are in principle similar to those for short chains.

c) The most probable r_{TF} distances for chains with different numbers of segments, L, depend only little on L in dense systems and are to a great degree predetermined by the radius of the sphere, R, (cf. also Fig. 1 in ref.[21]).

Results of our simulations suggest that long chains in dense systems are more coiled back towards tethered end than isolated tethered chains under the same external constraints (i.e. in the empty sphere of the same radius). The most probable chain conformations change fast with increasing numbers of chains (segment density) in the low

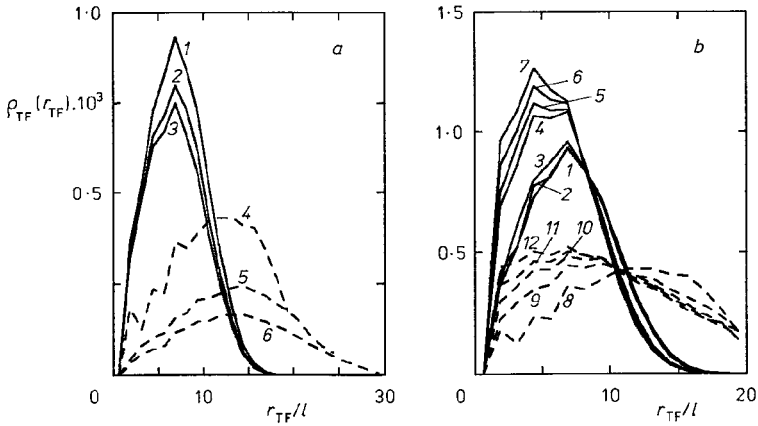

FIG. 5

Distribution functions $\rho_{TF}(r_{TF})$ for the following system: *a* an isolated tethered chain of the length, $L = 31$ (solid curves), in spherical cavities with $R = 10\ l$ (*1*), $R = 12.5\ l$ (*2*), $R = 15\ l$ (*3*); an isolated tethered chain of the length, $L = 93$ (dashed curves), in spherical cavities with $R = 10\ l$ (*4*), $R = 12.5\ l$ (*5*), $R = 15\ l$ (*6*); *b* multi-chain systems with chains of the length, $L = 31$ (solid curves) and $L = 93$ (dashed curves), in a spherical cavity with $R = 10\ l$ and increasing N, solid curves: $N = 1$, i.e. $g_S = 0.01$ (*1*), $N = 2$, $\langle g_S \rangle = 0.02$ (*2*), $N = 5$, $\langle g_S \rangle = 0.06$ (*3*), $N = 15$, $\langle g_S \rangle = 0.17$ (*4*), $N = 25$, $\langle g_S \rangle = 0.29$ (*5*), $N = 35$, $\langle g_S \rangle = 0.40$ (*6*), $N = 45$, $\langle g_S \rangle = 0.51$ (*7*) and dashed curves: $N = 1$, i.e. $\langle g_S \rangle = 0.03$ (*8*), $N = 5$, $\langle g_S \rangle = 0.17$ (*9*), $N = 10$, $\langle g_S \rangle = 0.34$ (*10*), $N = 15$, $\langle g_S \rangle = 0.51$ (*11*), $N = 20$, $\langle g_S \rangle = 0.68$ (*12*)

segment density region. At elevated segment densities, the end-to-end distribution functions do not almost depend on $\langle g_S \rangle$.

The presented results are in a good agreement with our previous observations[20–22] and with results of other authors[37,38] in the conclusion that the tethered chains in dense systems are preferentially stretched and radially oriented in systems with a low relative curvature, ξ, and disordered and more coiled in strongly curved (constrained) systems with a high ξ. This finding agrees also with a low scaling parameter $a \approx 0.33$ in the ln–ln plot of $\sqrt{\langle r_{TF}^2 \rangle}$ vs L that we have found in our earlier studies[21].

To complete the discussion of distributions of the end-to-end distances, $\rho_{TF}(r_{TF})$, we offer also the number fractions (Fig. 4*c* – insert) of chains with end-to-end distances, r_{TF}, for the systems presented in Fig. 4*c*, since it may be difficult for a reader to recalculate without other information the probability densities, $\rho_{TF}(r_{TF})$, to the number distribution functions, $n_{TF}(r_{TF})$.

Distributions of the tethered end-to-gravity center distances, $\rho_{TC}(r_{TC})$, for single chain systems with constant R, depend sensitively on L (Fig. 6*a* – 6*c*). With increasing number of segments, L, the most probable positions, $(r_{TC})_{max}$, increase significantly. "Tethered halves" of chains are generally less stretched in dense systems (insert in Fig. 6*c* – for systems with $R = 10\ l$), which is the result of a general tendency of chains in dense systems to fill in homogeneously the whole sphere with their segments[5,20,39].

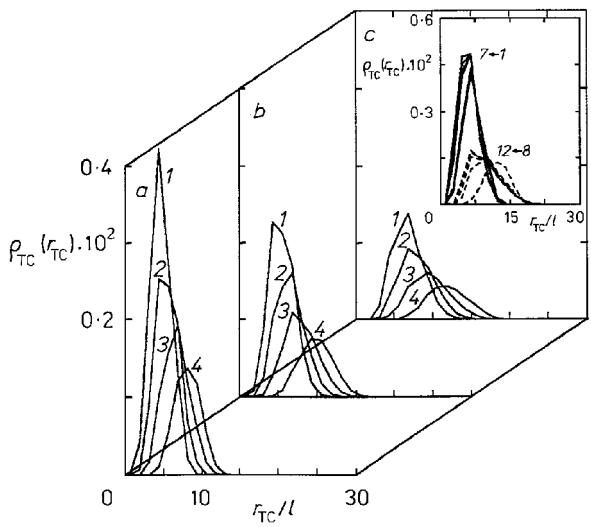

FIG. 6

Distribution function of the tethered end-to-gravity center distances, $\rho_{TC}(r_{TC})$, for the same systems containing a single tethered chain as in Fig. 4*a* – 4*c*; insert in Fig. 6*c* – distribution function, $\rho_{TC}(r_{TC})$, for the same multi-chain systems as in Fig. 5*b*, i.e. for $R = 10\ l$

In the studied systems, it is necessary to fill in a relatively large subsurfacial layer of the sphere.

Distributions of the free end-to-gravity center distances, $\rho_{FC}(r_{FC})$, for single chain systems are shown in Fig. 7*a* – 7*c*. Distributions for short chains (L = 31 in Fig. 7*a*) remind the "gaussian" distributions of the end-to-end distances for free and intersecting flexible chains. This "gaussian" shape has basically two reasons: (i) the "free halves" of chains are more flexible than the "tethered halves" and vectors $\boldsymbol{r}_{FC}$ are oriented almost at random in space, and (ii) the center of gravity of a chain does not usually coincide with a real chain segment and the exclusion principle does not therefore lower the probabilities for small $\boldsymbol{r}_{FC}$.

Distributions $\rho_{FC}(r_{FC})$ for single chains and high ξ show maxima for non-zero values of r_{FC} which may seem a bit surprising. One would expect a higher density of segments close to the gravity center for longer chains due in part to a higher chain flexibility and to a more important influence of external geometrical constraints. To explain the obtained curves, two functions: density of segments around the gravity center, $g_S^{(C)}(r_{CS})$, and the angular distribution of mutual orientations of $\boldsymbol{r}_{FC}$ and $\boldsymbol{r}_{TC}$ vectors, $n_{FC}^{(TC)}(\omega)$ (see the next subsection), have to be considered. Densities of segments, $g_S^{(C)}(r_{CS})$, around the gravity center (Fig. 7*c* – insert, for R = 15 l) for $r_{CS} \to 0$ decrease with increasing L. The shape of $\rho_{FC}(r_{FC})$, as well as the dependence of $g_S^{(C)}(r_{CS})$ on L may be accounted for

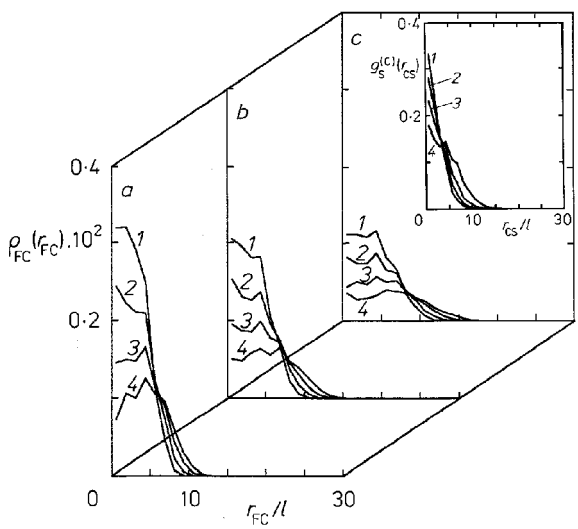

FIG. 7

Distribution function of the free end-to-gravity center distances, $\rho_{FC}(r_{FC})$, for the same systems as in Fig. 4; insert in Fig. 7*c* – the ensemble average density of segments in a single tethered chain around its gravity center, $g_S^{(C)}(r_{CS})$, for R = 15 l and L = 55 (*1*), L = 71 (*2*), L = 99 (*3*) and L = 163 (*4*)

by the assumption that the most probable conformation of a chain forms a "C-shaped" contour and the gravity center is shifted (mainly for long chains) outside the main cloud of chain segments. This assumption will be justified by discussing the mutual orientations of $\boldsymbol{r}_{FC}$ and $\boldsymbol{r}_{TC}$ vectors in the next subsection.

Orientational Distribution Functions

External geometrical constraints affect in the first place possible orientations of individual segments of a chain in space with respect to the tethered end. It is the reason why changes in angular distribution functions with increasing constraint parameter, ξ, and segment density, $\langle g_S \rangle$, are more obvious than changes in other distributions.

Figure 8 shows the angular distribution functions of orientations of the end-to-end vectors with respect to the radial direction, $\psi_{TF}^{(r)}(\vartheta)$, for the same systems as in Figs 4, 6 and 7. Distributions for systems with low constraint parameter, ξ, have a local minimum at low angles close to $\vartheta = 0°$, and reach maxima for $\vartheta \in \langle 50 - 60° \rangle$. Then they drop to low values for $\vartheta \to 90°$. Maximum close to 50 – 60° is a simple result of high numbers of possible arrangements of chains which reach with their free ends into the volume elements defined by a small angle difference, $\Delta\vartheta = 5°$, in the angular region, $\vartheta \in \langle 50°,60° \rangle$, i.e. into the volume elements, confined between two cones with the common apex which corresponds to the tethered end location at the spherical surface (the inner cone angle, ϑ, and the outer cone angle, $\vartheta + \Delta\vartheta$) – see Fig. 2. The

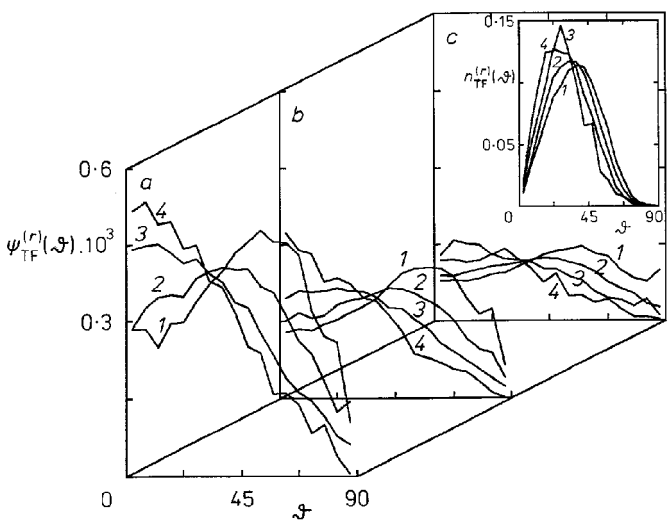

FIG. 8

Angular distribution function, $\psi_{TF}^{(r)}(\vartheta)$, of orientations of end-to-end vectors, $\boldsymbol{r}_{TF}$, with respect to the radial direction (angle ϑ) for the same systems as in Fig. 4; insert in Fig. 8*c* – number fractions, $n_{TF}^{(r)}(\vartheta)$, of chains corresponding to functions, $\psi_{TF}^{(r)}(\vartheta)$, in Fig. 8*c*

number fractions, $n_{TF}^{(r)}(\vartheta)$, corresponding to distribution functions, $\psi_{TF}^{(r)}(\vartheta)$, in Fig. 8*c*, are shown in the insert.

Long and severely constrained tethered chains in small closed volumes must adopt different conformations than short and less constrained tethered chains. The former prefer the longest possible r_{TF} distances and that requires an almost radial orientation of $\boldsymbol{r}_{TF}$ vectors into the most distant part of the sphere (i.e. into the opposite part with respect to the tethered end).

The most striking trends are depicted in Figs 9*a*, 9*b*. The basic shape of angular distribution functions, $\psi_{TF}^{(r)}(\vartheta)$, for less constrained systems, $\xi = 3.1$, $R = 10\ l$, does not change with increasing segment density, $\langle g_S \rangle$ (Fig. 9*a*). The only changes may be observed in positions and values of maxima. Both characteristics increase with increasing density of the system. For more constrained systems, $\xi = 9.3$, the situation is quite different. The curve shape changes completely with increasing $\langle g_S \rangle$, see Fig. 9*b*. A broad maximum close to $\vartheta = 0°$ which is typical for the low density region disappears at elevated densities and inverts into a local minimum. A new pronounced maximum appears in the angular region, $\vartheta \in \langle 50°,60° \rangle$. Segments of long chains in dense and constrained systems are forced to occupy a high and constant fraction of lattice points everywhere in the sphere[21,31,39]. Individual chains are therefore more coiled at higher densities. Average end-to-end distances, $\sqrt{\langle r_{TF}^2 \rangle}$, are shorter in comparison with those in the low density region, $\sqrt{\langle r_{TF}^2 \rangle} = 12.62\ l$ (for $N = 1$, $L = 93$, i.e. $\langle g_S \rangle = 0.03$), $\sqrt{\langle r_{TF}^2 \rangle} = 11.74\ l$ ($N = 10$, $L = 93$, $\langle g_S \rangle = 0.34$), $\sqrt{\langle r_{TF}^2 \rangle} = 11.54\ l$ ($N = 20$, $L = 93$, $\langle g_S \rangle = 0.68$) (see also Fig. 5). The free ends of highly coiled tethered chains are pref-

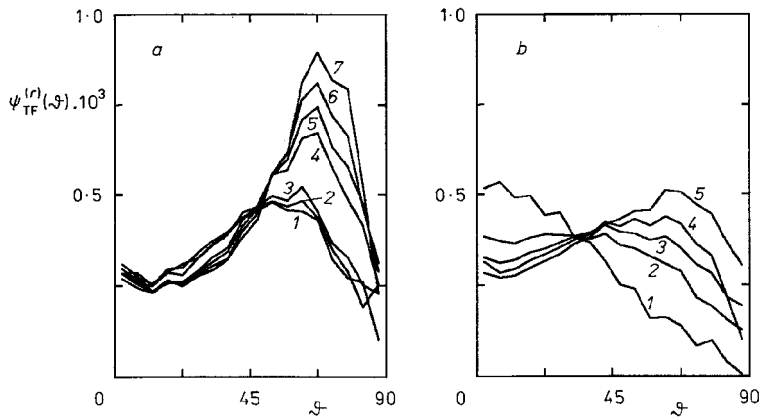

FIG. 9

Angular distribution functions, $\psi_{TF}^{(r)}(\vartheta)$, for multi-chain systems in a spherical cavity with the radius $R = 10\ l$: *a* $L = 31$; $N = 1$ (*1*), $N = 2$ (*2*), $N = 5$ (*3*), $N = 15$ (*4*), $N = 25$ (*5*), $N = 35$ (*6*), $N = 45$ (*7*); *b* $L = 93$; $N = 1$ (*1*), $N = 5$ (*2*), $N = 10$ (*3*), $N = 15$ (*4*), $N = 20$ (*5*)

erentially placed into angular-dependent volume elements with high numbers of lattice sites (see Fig. 2). Such multi-chain arrangements lead to the maximum entropy in dense systems of long tethered chains. Those systems are therefore highly disordered.

Very interesting information may be gained from a comparison of various angular characteristics concerning the orientations of the tethered end-to-gravity center and the free end-to-gravity center vectors, $\boldsymbol{r}_{TC}$ and $\boldsymbol{r}_{FC}$, respectively, and from their comparison with orientations of the tethered-to-free end vectors, $\boldsymbol{r}_{TF}$.

Figure 10 shows the angular distribution of orientations of the tethered end-to-gravity center vectors, $\psi_{TC}^{(r)}(\vartheta)$, with respect to the radial direction, for the same systems as in previous triplets of figures. The "tethered halves" are more influenced by the concave curvature of the surface and are effectively more rigid. The resulting directions of $\boldsymbol{r}_{TC}$ vectors are therefore confined in a narrower angular range than the corresponding $\boldsymbol{r}_{TF}$ vectors. Distributions for less constrained systems, $\xi = 3.1$, are almost uniform for $\vartheta \in$ <0°,45°> with a shallow minimum for $\vartheta \to 0°$ and an insignificant maximum close to $\vartheta \approx 40°$. All curves drop steeply for $\vartheta > 45°$. Distributions for highly constrained systems, $\xi = 9.3$, are quite narrow with well pronounced maxima for $\vartheta \to 0°$. They decrease fast in the angular region $\vartheta \in$ <20°,30°> and their values for $\vartheta > 30°$ are unimportant. The change in shape of $\psi_{TC}^{(r)}(\vartheta)$ with increasing ξ is similar to that in $\psi_{TF}^{(r)}(\vartheta)$. Curves $\psi_{TC}^{(r)}(\vartheta)$ for increasing numbers of chains, N, are shown in Fig. 11. At

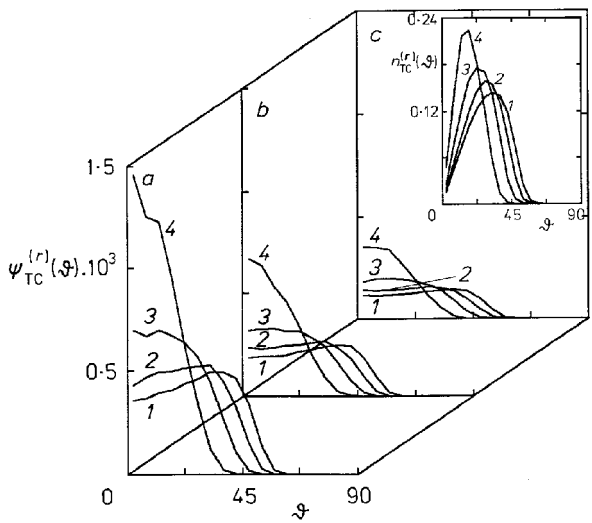

FIG. 10

Angular distribution function of orientations of $\boldsymbol{r}_{TC}$ vectors with respect to the radial direction, $\psi_{TC}^{(r)}(\vartheta)$, for the same systems as in Fig. 4, insert in Fig. 10*c* – number fractions, $n_{TC}^{(r)}(\vartheta)$, corresponding to $\psi_{TC}^{(r)}(\vartheta)$ in Fig. 10*c*

high segment densities, all curves are similar to each other and remind basically curve *1* in Fig. 10*a* with an evident minimum at low angles and a pronounced maximum for $\vartheta \in \langle 30°,40° \rangle$, depending on L.

Number fractions of orientations of the tethered end-to-gravity center vectors, $\boldsymbol{r}_{TC}$, with respect to the radial direction, $n_{TC}^{(r)}(\vartheta)$ (insert in Fig. 10*c* for chains in a cavity with $R = 15\ l$), and number fractions of orientations of the free end-to-gravity center vectors, $n_{FC}^{(r)}(\vartheta)$, in Fig. 12 (for all studied systems), show clearly that the angular orientations of the "tethered halves" of chains change both with ξ and $\langle g_S \rangle$, however those of the "free halves" do not (cf. also Fig. 7 in ref.[22] for high segment densities). As mentioned earlier, those curves (as well as the other functions) were calculated in a broad region of ξ and $\langle g_S \rangle$, but they are not shown here since we feel that the presented set of data is just at the limit of a reasonable size of a comprehensible paper.

Distributions of the angles, ω, between $\boldsymbol{r}_{FC}$ and $\boldsymbol{r}_{TC}$ vectors, $n_{FC}^{(TC)}(\omega)$, for single chain systems in a cavity with $R = 15\ l$, i.e. for $N = 1$ and $L = 55$ (curve *1*), $L = 72$ (*2*), $L = 93$ (*3*) and $L = 163$ (*4*) are shown in Fig. 13. These distribution functions (i.e. the number distribution of chains with corresponding ω) have very pronounced maxima close to 140° which suggests (together with the findings shown in Fig. 7) that the average conformation of a chain forms a "C-shaped cloud of segments".

Simulated distribution functions of projections of $\boldsymbol{r}_{TF}$, $\boldsymbol{r}_{TC}$ and $\boldsymbol{r}_{FC}$ vectors into the radial direction, $f_{TF}^{(r)}(p_{TF}^{(r)})$, $f_{TC}^{(r)}(p_{TC}^{(r)})$ and $f_{FC}^{(r)}(p_{FC}^{(r)})$, confirm conclusions drawn from the previous figures and are not shown here (they are available upon request). The "tethered halves" of chains are more influenced by both ξ and $\langle g_S \rangle$ than the "free halves". In systems with long chains, an increase in segment density provokes the preferential coiling of the "tethered halves" of chains.

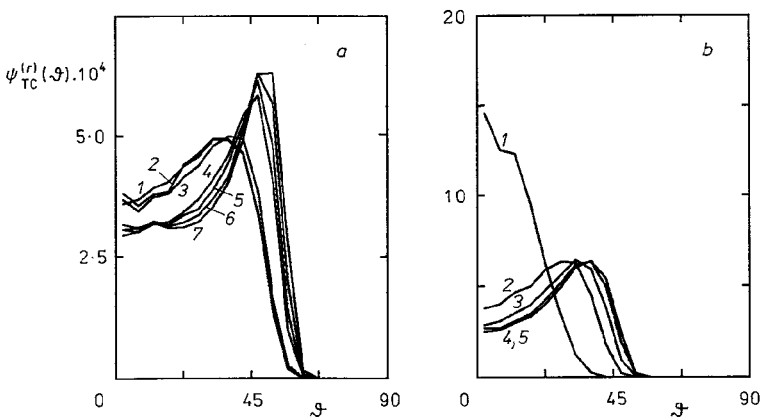

FIG. 11
Angular distribution function, $\psi_{TC}^{(r)}(\vartheta)$, for the same multi-chain systems as in Fig. 9

Persistence Properties

Figure 14 shows the number fractions of $\boldsymbol{r}_{TF}$ vectors oriented at angles φ with respect to the direction of the first-to-second segment connection, $n_{TF}^{(12)}(\varphi)$. The angular range of possible orientations covers generally $\varphi \in \langle 0°, \varphi_{max} \rangle$, with $\varphi_{max} < 180°$, depending on

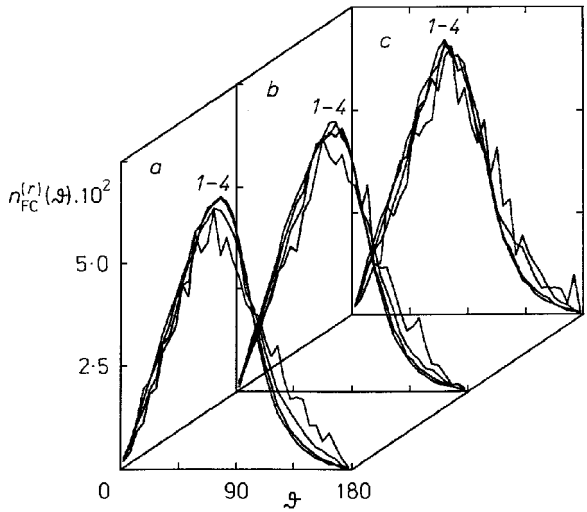

FIG. 12
Number fractions, $n_{FC}^{(r)}(\vartheta)$, of chains with orientations of $\boldsymbol{r}_{FC}$ vectors with respect to the radial direction (angle ϑ) for the same systems as in Fig. 4

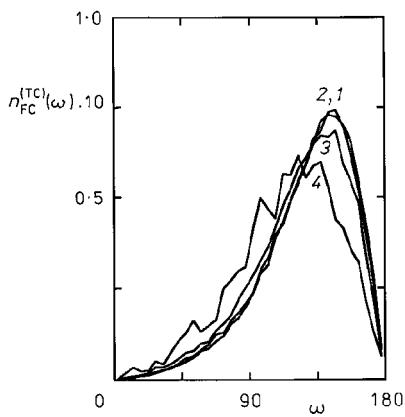

FIG. 13
Number fraction, $n_{FC}^{(TC)}(\omega)$, of chains with mutual orientations ω of the tethered end-to-gravity center vector, $\boldsymbol{r}_{TC}$, and the free end-to-gravity center vector, $\boldsymbol{r}_{FC}$, for the same systems as in Fig. 4*c*, i.e. for $R = 15$ *l*, $N = 1$ and $L = 55$ (*1*), $L = 71$ (*2*), $L = 99$ (*3*), $L = 163$ (*4*)

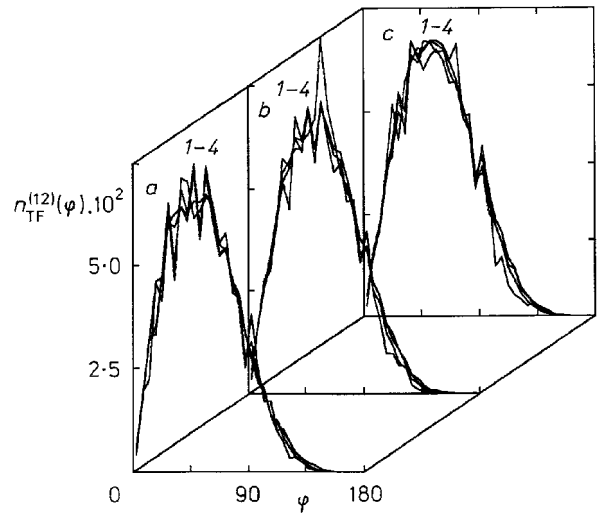

FIG. 14

Number fractions, $n_{TF}^{(12)}(\varphi)$, of chains with $\boldsymbol{r}_{TF}$ vectors oriented at the angle φ with respect to the direction of the first-to-second segment connection for the same systems as in Fig. 4

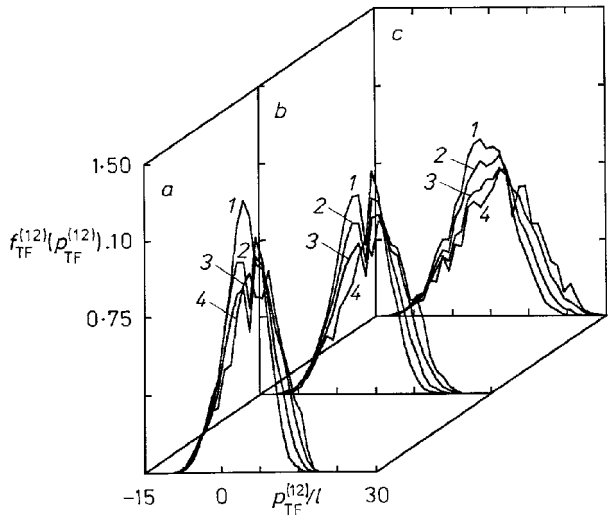

FIG. 15

Distributions, $f_{TF}^{(12)}(p_{TF}^{(12)})$, of projections of $\boldsymbol{r}_{TF}$ vectors into the direction of the first-to-second segment connection for the same systems as in Fig. 4

R/l (we show angles from 0 to 180°, since $n_{TF}^{(12)}(\varphi) = 0$, for $\varphi > \varphi_{max}$). All simulated curves are almost identical and coincide also with curves for dense systems (Fig. 11 in ref.[21]).

Distributions of projections of vectors $\boldsymbol{r}_{TF}$ into the direction of the first-to-second segment connections, $f_{TF}^{(12)}(p_{TF}^{(12)})$, Fig. 15, depend very little both on ξ and $<g_S>$, curves for chains with $L = 31$ and 93 do not almost change with $<g_S>$ and are not shown here. Individual distributions depend mainly on R. They are therefore very similar to those presented in ref.[22] for high segment densities. Simulated data for concave systems containing one, or just few tethered chains submitted to significant geometrical constraints confirm our assumption[21,22] that high values of the ensemble average, $<p_{TF}^{(12)}>$ (the persistence length), are mainly results of geometrical constraints imposed by the surface to which the chain ends are tethered and which cannot be crossed. The presence of that surface in the studied systems prevents the spatial randomization of chain conformations (i.e. the angular randomization of $\boldsymbol{r}_{TF}$ orientations) around the first segment. Relatively small closed volumes of all studied systems limit on the other hand the longest possible projections, $p_{TF}^{(12)}$, and the simulated distribution functions, $f_{TF}^{(12)}(p_{TF}^{(12)})$, reach pronounced maxima in a relatively narrow range of $p_{TF}^{(12)}$ which depend only little on ξ.

Radii of Gyration and Scaling Properties

The last section concerning the low density region is particularly interesting for comparison of simulated data with systems of free chains. Figures 16 and 17 show distributions of radii of gyrations, $g_R(R_g)$, for the same systems as in Figs 4 and 5, respectively.

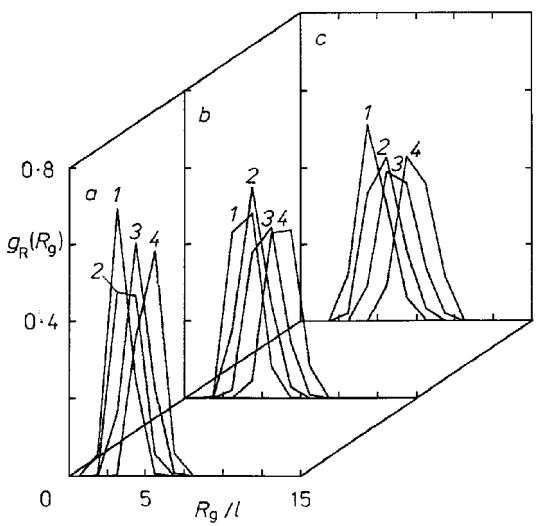

FIG. 16
Distribution of the radii of gyration of individual chains, $g_R(R_g)$, for the same systems as in Fig. 4

For low geometrical constraints, distribution functions of radii of gyration, $g_R(R_g)$, and the corresponding average values, $\langle R_g \rangle$, do not change with increasing $\langle g_S \rangle$. In systems with a high constraint parameter, $\xi = 9.3$, the radius of gyration decreases fast with increasing $\langle g_S \rangle$ and reaches soon a value which depends mainly on R and L, but not on $\langle g_S \rangle$.

Figure 18 depicts the ln–ln plot of $\langle R_g \rangle$ vs the chain length, L, in the low density region (for one tethered chain only). Curves *1*, *2* and *3* correspond to the cavity radius, R = 10 l, 12.5 l and 15 l, respectively. The scaling parameter, $a = 0.42 \pm 0.05$, for constraints, $\xi \approx 3 - 10$, depends only little on R and does not almost differ from that for dense systems (ref.[21]). The scaling of $\langle R_g \rangle$ does not depend on the average segment density, but the pre-exponential factor does. The ln $\langle R_g \rangle$ – ln L plot in a broader range of constraint parameters, $\xi \in \langle 1.0 - 10.9 \rangle$, is shown in the insert (for R = 15 l). In such a broad region of ξ (i.e. also L), the plot is not linear which is not surprising. Short chains with L = 15 are stiff and relatively stretched, while the long chains with L = 163 are more flexible and must be more coiled in a cavity of the radius R = 15 l.

Concluding General Remarks Concerning the Low Density Region

A quite extensive collection of simulated data for one tethered chain under various geometrical constraints, ξ, together with data for systems of many tethered chains in a broad range of segment densities, $\langle g_S \rangle$, enabled us to analyze various aspects of the conformational behavior of a single tethered and constrained chain and the relationship between dilute and dense systems. A detailed discussion of various distribution functions allows for a complex description of many properties of tethered chains in constrained volumes.

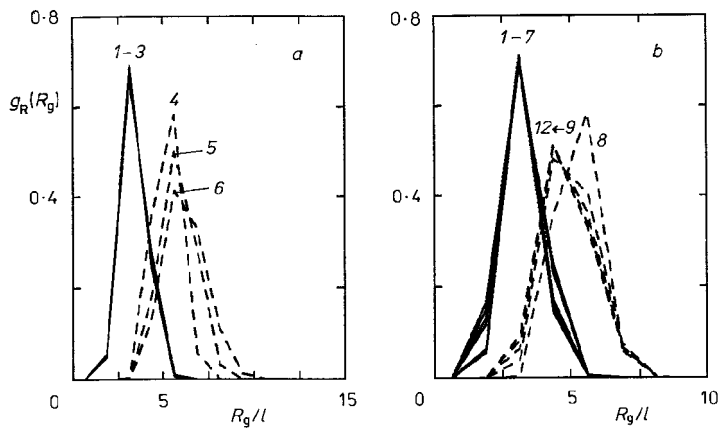

FIG. 17
Distribution of the radii of gyration of individual chains, $g_R(R_g)$, for the same systems as in Fig. 5

Conformational characteristics of dilute systems of tethered chains submitted to low constraints in relatively large spherical volumes remind basically those of an isolated free self-avoiding chain (it concerns those characteristics which are meaningful to compare) if we do not require the spherical symmetry of distribution functions with respect to the tethered end. Relatively long chains in highly constrained systems must adopt altered conformations which differ from those of free self-avoiding chains.

An orientational effect of the surface on the segment arrangements decays fast in the chain segment succession from the tethered end towards the free end: the performed simulations indicate that vectors $\boldsymbol{r}_{TC}$ are partially oriented, whereas vectors $\boldsymbol{r}_{FC}$ are uniformly distributed in all possible directions even for relatively short chains.

In dense multi-chain systems, individual chains are forced to occupy a high and uniform fraction of lattice sites in the whole sphere. The "tethered halves" of chains are more coiled and a high fraction of $\boldsymbol{r}_{TC}$ vectors decline from the radial direction. The dense systems with long chains are generally highly disordered.

Almost all distributions depend on $\langle g_S \rangle$, however we have not detected any indication of the behavior of individual chains approaching the "ideal chain behavior" (i.e. that of an intersecting chain) which is known for dense systems of free self-avoiding chains[30,31]. This finding is not surprising since external geometrical constraints play a more important role than the other factors (e.g. segment density etc.).

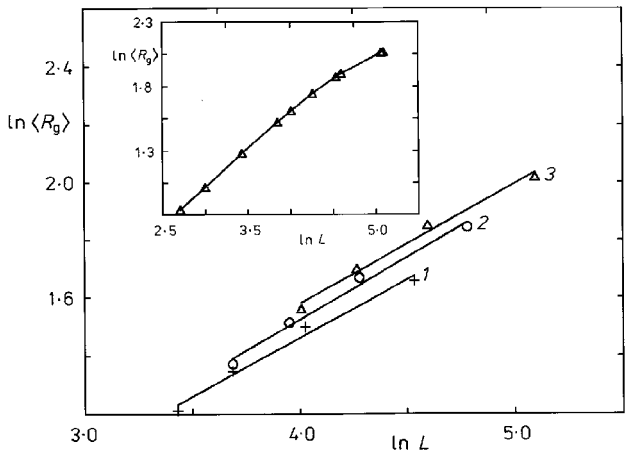

FIG. 18
The ln $\langle R_g \rangle$–ln L plot for systems containing one tethered chain in spherical cavities with $R = 10\ l$ (*1*), $R = 12.5\ l$ (*2*), $R = 15\ l$ (*3*)

Studies of the Applicability of our Simulation Procedure for Highly Dense Systems

It is well known fact that the self-avoiding walk algorithm does not work well at elevated segment densities and breaks down completely at high densities (an average fractions of the occupied lattice sites ≈ 0.7). We have found earlier that the "crankshaft--motion" algorithm[36] is only little efficient in systems of tethered chains[20] in small volumes even at relatively low segment densities ≈ 0.3. Simulation techniques, such as "reptation" algorithm[40,41], etc. cannot be used for tethered chains and the "bond-breaking" algorithm[42,43] would violate the monodispersity of chains in our system. We use the Frenkel and Siepmann[34] modification of the self-avoiding walk algorithm which was found suitable for dense systems of free chains. We were able to go up to quite high densities (depending on the combination of N and L – it works better for combinations of lower N with higher L values than for inverse combinations of higher N with lower L). In the high density region, the simulation time increases considerably, since a very high fraction of multi-chain arrangements are forbidden. Figure 19 shows an average CPU time necessary for a successful simulation of one micelle for $R = 10\ l$, $N = 25$ and increasing number of segments, L, as a function of the average segment density, $\langle g_S \rangle = NL/N_{tot}$. It is evident that in a relatively narrow region of $\langle g_S \rangle \in \langle 0.65, 0.70 \rangle$, the simulation time starts to grow up very steeply.

We were concerned if this sudden increase in the computational time means:

a) Only a decreasing efficiency of the used simulation procedure,

b) a fatal break-down of the computational efficiency which prevents the proper equilibration of the system in a finite time, or

c) a real physical change in the conformational behavior of the system.

We have performed a series of time-consuming simulations to investigate the above described problem. Simulations for medium density systems ($\langle g_S \rangle \in \langle 0.5 - 0.6 \rangle$) comparing the modified and the original algorithm have shown that the new version of

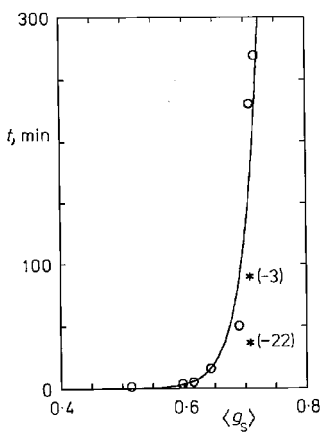

FIG. 19

Average CPU time necessary to simulate one multi-chain system containing a constant number, $N = 25$, of tethered chains with increasing chain length, L, in a spherical cavity with $R = 10\ l$ as a function of $\langle g_S \rangle$. Points with (–3) and (–22) give CPU time for the upgraded algorithm using an initial simultaneous self-avoiding walk with chains of the length $(L - 3)$ and $(L - 22)$, respectively

the simulation program gives equivalent data with the old version in a considerably shorter time.

All distribution functions obtained with the upgraded algorithm for high density systems ($<g_S> > 0.6$) are practically identical with those based on the original algorithm. Small changes and their trends accompanying an increase in density into the region, which we could not study with the original algorithm, are gradual and smooth. They cannot be classified as sudden and physically meaningful changes in shape of distribution curves. Simulated data show that a significant loss of the computational efficiency at high segment densities is an inherent feature of our simulation technique (similarly to all simulations based on the random self-avoiding walk algorithm). However, the upgraded algorithm allows to get well equilibrated data even for highly dense systems, i.e. up to $<g_S>$ ca 0.75. Simulation time increases considerably for densities higher than 0.6, and the rise in CPU time is very steep and sudden, but no significant changes in conformational characteristics with increasing $<g_S>$ were observed. We believe that the data obtained for $<g_S> \in <0.5 - 0.75>$ describe qualitatively well the behavior of the dense system of tethered chains in small spherical volumes at high densities, even for $<g_S> \to 1$.

CONCLUSIONS

1. Computer simulations of conformational characteristics (distribution functions of end-to-end distances, $\rho_{TF}(r_{TF})$, end-to-gravity center distances, $\rho_{TC}(r_{TC})$ and $n_{FC}(r_{FC})$, etc., angular distribution functions of orientations of end-to-end vectors $\psi_{TF}^{(r)}(\vartheta)$, with respect to the radial direction, etc., distributions of projections of various vectors into the selected directions, radii of gyration, etc.) were performed for systems of tethered chains in small closed volumes for various numbers of chains, N, numbers of segments, L, and increasing radii of spherical cavities, R.

2. A special attention was focused on two limiting density regions: (i) the low density limit (i.e. a single tethered chain in the cavity), and (ii) the high density region, $<g_S>$ ca 0.5 – 0.75. Changes in various structural characteristics with increasing density and constraint parameter, $\xi = Ll/R$, were studied.

3. Properties of significantly constrained tethered chains ($\xi \approx 6 - 10$) depend sensitively both on $<g_S>$ and ξ, whereas most of structural characteristics of less constrained systems ($\xi \approx 3 - 4$) depend only little on $<g_S>$ and do not depend at all on ξ.

4. Behavior of all studied systems is quite complex. Tethered chains in multi-chain systems are more stretched and partially radially oriented at low constraints (i.e. in systems with a low relative curvature, $\xi = Ll/R$), and more coiled and disordered at high ξ.

5. The upgraded version of the simulation procedure allows to study really dense systems of tethered chains ($<g_S> \approx 0.75$) – in that case, the simulation time, necessary to get well equilibrated data, increases very fast with increasing density.

This work was supported by Grants No. 203/93/2287 and No. 203/94/0693 (Grant Agency of the Czech Republic).

REFERENCES

1. Alexander S.: J. Phys. France *38*, 983 (1977).
2. Wijmans C. M., Scheutjens J. M. A. M., Zhulina E. B.: Macromolecules *25*, 2657 (1992).
3. Bauer B. J., Fetters L. J., Graessley W. W., Hadjichristidis N., Quack G. F.: Macromolecules *22*, 2337 (1989).
4. Batoulis J., Kremer K.: Europhys. Lett. *7*, 683 (1988).
5. Tuzar Z., Kratochvil P. in: *Surface and Colloid Science* (E. Matijevic, Ed.), Vol. 15, p. 1. Plenum Press, New York 1993.
6. Nagarajan R., Ganesh K.: J. Chem. Phys. *90*, 5843 (1989).
7. Rouse P. E.: J. Chem. Phys. *21*, 1272 (1953).
8. Smit B., van der Put A., Peters J. C., de Swaan Arons J., Michels J. P. L.: J. Chem. Phys. *88*, 3372 (1988).
9. Grest G. S., Kremer K., Milner S. T., Witten T. A.: Macromolecules *22*, 1904 (1989).
10. Halperin A., Tirrell M., Lodge T. P.: Adv. Polym. Sci. *100*, 31 (1991).
11. Allen M. P., Tildesley D. J.: *Computer Simulations of Liquids*. Clarendon Press, London 1986.
12. Kremer K., Binder K.: Comp. Phys. Rep. *7*, 259 (1988).
13. Binder K., Heerman D. W.: *Monte Carlo Simulation in Statistical Physics 80, Springer Series in Solid State Physics*, p. 10. Springer, Berlin 1988.
14. Kremer K., Grest G. S.: J. Chem. Soc., Faraday Trans. *88*, 1707 (1992).
15. Kremer K., Grest G. S.: J. Chem. Phys. *92*, 5057 (1990).
16. Murat M., Grest G. S.: Macromolecules *24*, 704 (1991).
17. Rodrigues K., Mattice W.: J. Chem. Phys. *94*, 761 (1991).
18. Wang Y., Mattice W. L., Napper D. H.: Macromolecules *25*, 4073 (1992).
19. Wang Y., Mattice W. L., Napper D. H.: Langmuir *9*, 66 (1993).
20. Limpouchova Z., Prochazka K.: Collect. Czech. Chem. Commun. *58*, 2290 (1993).
21. Prochazka K., Limpouchova Z.: Collect. Czech. Chem. Commun. *59*, 782 (1994).
22. Limpouchova Z., Prochazka K.: Collect. Czech. Chem. Commun. *59*, 803 (1994).
23. Prochazka K., Limpouchova Z., Munk P., Webber S. E.: J. Fluorescence, in press.
24. Gochanour C. R., Andersen H. C., Fayer M. D.: J. Chem. Phys. *70*, 4254 (1979).
25. Loring R. F., Andersen H. C., Fayer M. D.: J. Chem. Phys. *76*, 2015 (1982).
26. Prochazka K., Kiserow D., Ramireddy C., Tuzar Z., Munk P., Webber S. E.: Macromolecules *25*, 454 (1992).
27. Kiserow D., Prochazka K., Ramireddy C., Tuzar Z., Munk P., Webber S. E.: Macromolecules *25*, 461 (1992).
28. Prochazka K., Bednar B., Mukhtar E., Svoboda P., Trnena J., Almgren M.: J. Phys. Chem. *95*, 4563 (1991).
29. Prochazka K., Medhage B., Mukhtar E., Almgren M., Svoboda P., Trnena J., Bednar B.: Polymer *34*, 101 (1993).
30. de Gennes P. G. in: *Solid State Physics* (J. Liebert, Ed.), Suppl. 14, p. 1. Academic Press, New York 1978.
31. de Gennes P. G.: *Scaling Concepts in Polymer Physics*. Cornell University, Ithaca 1979.
32. Rosenbluth M. N., Rosenbluth A. W.: J. Chem. Phys. *23*, 356 (1955).

33. Metropolis N., Rosenbluth A. W., Rosenbluth M. N., Teller A., Teller H.: J. Chem. Phys. *21*, 1087 (1953).
34. Siepmann J. I., Frenkel D.: Mol. Phys. *75*, 59 (1992).
35. Verdier P. H., Stockmayer W. H.: J. Chem. Phys. *36*, 227 (1962).
36. Grest G. S., Murat M.: Macromolecules *26*, 3108 (1993).
37. Ball R. C., Marko J. R., Milner S. T., Witten T. A.: Macromolecules *24*, 693 (1991).
38. Perahia D., Weisler D., Satija S. K., Fetters L. J., Sinha S. K., Milner S. T.: Phys. Rev. Lett., in press.
39. Cheng P.-L., Berney C. V., Cohen R. E.: Macromolecules *21*, 3442 (1988).
40. Kron A. K., Ptitsyn O. B., Skvortsov A. M., Fedorov A. K.: Mol. Biol. *1*, 486 (1967).
41. Wall T. F., Mandel F.: J. Chem. Phys. *63*, 4592 (1975).
42. Mansfield M. L.: J. Chem. Phys. *77*, 1554 (1982).
43. Madden W. G.: J. Chem. Phys. *87*, 1405 (1987).

Translated by the author (K. P.).